Lindt, Kevin; Mattea, Carlos; Stapf, Siegfried; Ostrovskaya, I. K.; Fatkullin, Nail F.

The Deuteron NMR Hahn Echo Decay in Polyethylen oxide melts

Original published in: AIP Advances / American Institute of Physics. - New York, NY : American Inst. of Physics. - 12 (2022), 7, art. 075219, 12 pp.

Original published: 2022-07-29

ISSN: 2158-3226

DOI: 10.1063/5.0099293

[*Visited:* 2022-09-29]

The deuteron NMR Hahn echo decay in polyethylene oxide melts

Cite as: AIP Advances 12, 075219 (2022); doi: 10.1063/5.0099293
Submitted: 16 May 2022 • Accepted: 27 June 2022 •
Published Online: 29 July 2022

View Online Export Citation CrossMark

K. Lindt,[1,a)] C. Mattea,[1] S. Stapf,[1] I. K. Ostrovskaya,[2] and N. F. Fatkullin[2]

AFFILIATIONS

[1] Department Technical Physics II/Polymer Physics, TU Ilmenau, P.O. Box 100 565, D-98684 Ilmenau, Germany
[2] Institute of Physics, Kazan Federal University, Kazan 420008, Tatarstan, Russia

[a)] **Author to whom correspondence should be addressed:** kevin.lindt@tu-ilmenau.de

ABSTRACT

The deuteron transverse relaxation properties of polyethylene oxide melts of four different molecular weights, covering the range from the onset of entanglements to the regime of fully entangled chains, are investigated using Hahn echo decays over an extensive time interval up to ten times the effective transverse spin relaxation time. The results are compared to predictions based on the Rouse and reptation formalisms, taking into account the dynamical heterogeneity of linear polymer chains produced by the end segments. The experimental results can be described qualitatively by a combination of both models, with the contribution of reptation dynamics increasing with growing chain length. The transition is continuous, rather than being characterized by sharp regime boundaries. Up to a molecular weight of 300.000 g/mol, the predicted limit of pure reptation dynamics is not yet reached. Quantitative deviations from the predicted decays as computed by numerical procedures become observable toward the long-time limit of the Hahn echo decays and are being discussed in terms of shortcomings of the available reptation theories.

I. INTRODUCTION

Nuclear Magnetic Resonance (NMR) has traditionally been a powerful approach to verify and improve dynamic models of polymer dynamics in the melt state, the best-known concepts of which are represented by the Rouse model for short and unentangled chains, and the reptation model for long and multiple entangled molecules (see, for example, Refs. 1–6 and articles cited therein). In the most general terms, the essence of the various NMR methods is that the spin subsystem of the substance under study, which is initially in a state of thermodynamic equilibrium, is manipulated by a particular sequence of radiofrequency pulses and measures the dynamic response of the system to this influence. The time dependence of the measured signal depends on the nature of spins' fluctuations in space. Therefore, the measured signal can be expressed through dynamic correlation functions, which, on the other hand, can be theoretically predicted based on existing dynamic models. A comparison of experimental data with theoretical predictions, in turn, provides a basis for improving our understanding of the dynamics and structure of the systems under study.

The Hahn echo (HE) is one of the technically simplest methods of pulsed NMR methods, which have been used for decades in the experimental investigation of polymer dynamics (see, for example, Refs. 7–14). It is the response of spins of the investigated system on two radiofrequency pulses. The experiment begins with a defined situation of all spins contained in the sample being placed in a temporarily constant magnetic field oriented, by definition, along the z axis and being in their thermodynamic equilibrium state, i.e., with the total magnetization oriented along z and assuming the Curie equilibrium value. Following an initial resonant radiofrequency pulse, $P_x^{\pi/2}$ as written in its operator representation, the magnetization is rotated by an angle of $\pi/2$ relative to the x axis, so that a non-equilibrium state of the spin system is created. Following a time interval τ, the spin system is irradiated by a second radiofrequency pulse P_x^{π} rotating the magnetization by the angle π relative to the x axis. The experimentally observed response of the spin system on the two described radiofrequency pulses at time moment $t = 2\tau$ is named the Hahn echo. After the first pulse $P_x^{\pi/2}$, the so-called Free Induction Decay (FID) is observed, caused by the

precession of the non-equilibrium magnetization around the magnetic field, which induces an oscillating voltage in the receiver coil. The FID decays, on the one hand, by dephasing due to the distribution of Larmor frequencies either by inhomogeneous magnetic fields within the sample volume or by the multiplicity of chemical shifts and, on the other hand, by fluctuations in the internal electromagnetic fields that allow spin transitions and are modulated by the molecular motions that affect the spin system. The latter effect is called NMR relaxation in its proper sense. While the dephasing effect may be neglected for short evolution times under favorable conditions, such as the high homogeneity typically achieved in commercial NMR spectrometers and in substances possessing only a single chemically distinct spin with one single chemical shift, the actual signal decay due to molecular motions can be isolated by compensating this dephasing effect using the Hahn echo. The decaying part of it is fully equivalent to the initial FID. For observation times exceeding the inverse of the Larmor frequency spread by either inhomogeneous fields or chemical shift differences, a Hahn echo or a similar echo sequence will be the method of choice. This paper will present the original experimental results obtained by the Hahn echo method, so, henceforth, we will discuss about it considering, by default, that the Hahn echo is completely analogous to the FID for a system of equivalent spins in a perfectly homogeneous magnetic field.

Possibilities of modern NMR spectrometers allow for experimental investigation of the Hahn echo over a period of time corresponding to a signal decay to at least 10^{-3}–10^{-4} times of the initial HE magnitude. However, the theoretical interpretation of the HE on such a long period of time will, at least in polymer melts, meet difficulties of a principal character that are connected to the still unresolved many-body problem of statistical mechanics. In fact, in polymer melts, a theoretically justified and analytically tractable approximation can be formulated only for shorter time periods $t < T_2^{\text{eff}}$, where T_2^{eff} is the effective spin–spin relaxation time defined by the relation $g\left(T_2^{\text{eff}}\right) = e^{-1}$, with $g(t)$ being the normalized HE signal at time moment $t = 2\tau$ and the condition $g(0) = 1$ (see, for example, Refs. 15–19). Within this time range, it is possible to limit the consideration to calculations of the second moment of magnetization, dependent on dynamic lattice pair-correlation functions. Higher-order moments, in addition to becoming cumbersome to compute, also contain higher-order dynamic correlation functions, which make them analytically intractable today. A common extrapolation to long times in such situations is the so-called Anderson–Weiss approximation, i.e., a second cumulant approximation based on the assumption that all higher-order moments can be expressed through the second moment. In essence, this means that in the general situation, the Anderson–Weiss approximation is theoretically justified within the same time limits as the second moment approximation. In our recent studies,[20–22] it has been shown that for the case of the tube-reptation model, assuming the central role in modern treatments of polymer melt dynamics, the description can, indeed, be extended beyond the Anderson–Weiss approximation if the time dependence of the HE for deuteron spins is considered, the relaxation of which is mainly determined by intramolecular interactions.

The main purpose of this article is to investigate experimentally the HE in deuterated melts of well-defined polyethylene oxides with different molecular masses as a function of temperature and to attempt a quantitative interpretation in terms of the above-mentioned approach.

II. THEORY

In this section, we will provide the necessary information related to the theory of the dynamics of macromolecules, adhering to the terminology and notation of the classical monograph.[23] In accordance with the phenomenological tube-reptation model, which is currently the dominating concept in the theory of macromolecular dynamics in polymer melts with sufficiently large molecular masses $N \gg N_e$—where N is the number of Kuhn segments per macromolecule and N_e is a phenomenological number treated as the average number of Kuhn segments between two entanglements[23]—the spatial displacement of macromolecules takes place inside "tubes" formed by the surrounding medium with the diameter $a = bN_e^{1/2}$, where b is the Kuhn segment length of polymer chains. The discussed model contains four characteristic time scales: the segmental relaxation time τ_s, the entanglement time $\tau_e = \tau_s N_e^2$, the Rouse relaxation time $\tau_R = \tau_s N^2$, and the tube disengagement, or terminal relaxation, time $\tau_d = 3\tau_R Z = 3\tau_e Z^3$, with the number of entanglements per chain $Z = N/N_e$. In accordance with these time scales, the following regimes of motions are distinguished:

1. Regime I, or *Rouse* (non-entangled) *regime* of motions, for the interval $t \ll \tau_e$, where polymer chains are moving in accordance with the Rouse model (see details, for example, in Refs. 23–27).
2. Regime II, or regime of *incoherent reptation*, for the interval $\tau_e \ll t \ll \tau_R$. Due to the entanglements between different polymer chains, each chain effectively becomes confined inside a tube with diameter a and performs one-dimensional anomalous Rouse diffusion with an exponent 1/2 for the time dependence of mean squared displacements inside their own tube. In this regime, parts of the chain that are sufficiently separated, i.e., by more than $\sqrt{t/\tau_s}$ segments along the chain, are moving independently from each other. The total mean squared displacement of polymer segments in space is changed here as $\langle r^2(t)\rangle \sim b^2 N_e^{1/2}(t/\tau_s)^{1/4}$. The length of the tube is computed as $L_T = aZ = bNN_e^{-1/2}$. The central line of the tube, the so-called primitive path, can be considered as an ideal chain constructed from primitive segments of length a.
3. Regime III, or regime of *coherent reptation*, for the interval $\tau_R \ll t \ll \tau_d$. The polymer chains still remain confined in their initial tubes, but perform normal one-dimensional Rouse diffusion inside the tube, when different polymer segments are moving coherently with each other and the mean square displacement inside the tube is proportional to time with total mean squared displacement $\langle r^2(t)\rangle \sim b^2 Z^{-1/2}(t/\tau_s)^{1/2}$.
4. Regime IV, or regime of normal diffusion, for the interval $t \gg \tau_d$. The polymer chains escape from their initial tubes and perform normal (Gaussian) diffusion with the diffusion coefficient $D_{cm} = \frac{1}{3\pi^2}\frac{Nb^2}{\tau_d} = \frac{1}{9\pi^2}\frac{b^2 N_e}{\tau_s N^2} = \frac{1}{9\pi^2}\frac{a^2}{\tau_e Z^2}$.

Note also that in the tube-reptation model, all polymer chains are considered as ideal chains, which seems to be an acceptable approximation for polymer melts in the light of Flory's ideality

hypothesis (see, for example, Refs. 23–26). Given a polymer chain consisting of N Kuhn segments, it can also be viewed as consisting of N/Z primitive segments, each of which contains N_e ordinary Kuhn segments. Since $N_e \gg 1$, any primitive segment of the polymer chain can be considered as an ideal Gaussian chain with the mean-squared length of the primitive segment $a^2 = b^2 N_e$.

In this work, due to the limitations of the experimental procedure, we are mainly interested in regimes II and III. The curvilinear mean-squared displacement inside the tube of polymer segments at corresponding times can be approximated by the following expression:[28]

$$\langle s^2(t)\rangle = \frac{2a^2}{3\pi^{3/2}}\left(\frac{t}{\tau_e}\right)^{1/2}\frac{1}{1+\frac{6}{\pi^{3/2}}\frac{1}{Z}\left(\frac{t}{\tau_e}\right)^{1/2}} + \frac{2}{3\pi^2}\frac{a^2}{Z}\frac{t}{\tau_e}. \quad (1)$$

The normalized HE amplitude of ^{2}H spins [i.e., $g^D(t=0) = 1$] at times $t \gg \tau_s$ can be represented through the spatial orientations of Kuhn segments by the following relation (see, for example, Refs. 11, 12, and 18):

$$g^D(t) = \frac{1}{N}\sum_k \mathrm{Re}\left\langle \exp\left\{ i\omega_Q \int_0^t dt_1 \left(3\cos^2(\theta_k(t_1)) - 1\right)\right\}\right\rangle, \quad (2)$$

where ω_Q is the intensity of quadrupole interaction expressed in frequency units, $\theta_k(t_1)$ is the angle between the vector connecting the ends of the segment of number k and the direction of the external magnetic field at time moment t_1, and $\langle\cdots\rangle$ represents the average over all stochastic trajectories of the polymer chains during the experimentally investigated time interval t. The quadrupole coupling constant in frequency units ω_Q in expression (2) is related to the quadrupole coupling constant $\frac{e^2qQ}{2\pi\hbar^2}$, which is contained in the Hamiltonian of the spin–lattice and spin–spin interactions, where eQ is the quadrupole moment of the nucleus and eq is the electric field gradient at the location of the nucleus (see, for example, Refs. 15–19). Our ω_Q is proportional to this quantity, $\omega_Q = \alpha_{s-s}\sqrt{\frac{5}{2}}\frac{3}{4}\frac{e^2qQ}{\hbar^2}$, where $\alpha_{s-s} < 1$ is a constant taking into account the fast intrasegmental motions averaging the major part of quadrupole interactions at times $t \gg \tau_s$. The numerical factor $\alpha_{s-s} < 1$ is not easily calculated from the first principles; therefore, we will consider ω_Q as a fitting parameter. This, of course, leaves the question about the actual meaning of a numerical coefficient such as α_{s-s} that, in the end, is obtained from comparing an expression with the experimental data. We will adhere, as in previous studies, to the following strategy: we will keep all the numerical coefficients that can be calculated exactly or estimated with sufficient accuracy. In the end, we will always be able to examine their importance by comparing the calculations with experimental results.

In the tube-reptation model, it is assumed that at times $t \le \tau_e$, the polymer segments carry out the fast fluctuations inside the tube about their primitive paths. At temperatures when the polymer is in the molten state, in all realistic experimental conditions, the entanglement time $\tau_e \ll T_2^{eff}$, allowing to rewrite expression (2) as follows:[22]

$$\begin{aligned} g^D(t) &= g^D_{fast}(t)\, g^D_{tb}(t) \\ &= \exp\left(-\frac{t}{T_2^{fast}}\right)\frac{1}{Z} \\ &\quad\times \sum_{k=1}^{Z}\mathrm{Re}\left\langle \exp\left\{ i\tilde{\omega}_Q \int_0^t dt_1 \left(3\cos^2(\theta_k(t_1)) - 1\right)\right\}\right\rangle_{rep}, \end{aligned} \quad (3)$$

where

$$g^D_{fast}(t) = \exp\left(-\frac{t}{T_2^{fast}}\right) \quad (4)$$

is the factor connected with the fast fluctuations of polymer segments inside the tube and

$$g^D_{tb}(t) = \frac{1}{Z}\sum_{k=1}^{Z}\mathrm{Re}\left\langle \exp\left\{ i\tilde{\omega}_Q \int_0^t dt_1 \left(3\cos^2(\theta_k(t_1)) - 1\right)\right\}\right\rangle_{rep} \quad (5)$$

is the factor connected with reptation motions along the primitive path. The time T_2^{fast} is expected to be of the order of the effective spin–spin relaxation time in polymer melts with a molecular mass measured in units of Kuhn segments of about N_e, and is, in situations where $N \gg N_e$, much longer than the corresponding $T_2^{eff}(N)$, i.e., $T_2^{fast} \approx T_2^{eff}(N_e) \gg T_2^{eff}(N \gg N_e)$.

In our recent work,[21] the HE of deuteron spins in non-entangled polymer melts, i.e., with molecular masses $N \le N_e$, was considered in the light of the dynamical heterogeneity of linear polymer chains, i.e., taking into account the end effects (some additional materials connected with the influence of dynamical heterogeneity on NMR spin relaxation can be found in the literature[29–33]). Assuming that the chains under these conditions are moving as Rouse chains, it was shown that the time dependence of the HE can be represented in the notation of this paper by the following relation:

$$\begin{aligned} g^D_{Rouse}(t) &= \frac{2}{N}\sum_{n\le\frac{N}{2}}\exp\left(-\frac{t}{\tilde{T}^R_{2,n}}\right), \\ \text{with } \frac{1}{\tilde{T}^R_{2,n}} &= \frac{4\pi}{9}\omega_Q^2\tau_s\,\ln(2\pi n). \end{aligned} \quad (6)$$

This case takes into account a distribution of the spin–spin relaxation times $\tilde{T}^R_{2,n}$: spins located at different segments have different relaxation times, i.e., the faster relaxing spins are in the central regions of the chain. The dependence of the relaxation times $\tilde{T}^R_{2,n}$ is logarithmic, and the initial rate of decay is approximately

$$\frac{1}{\tilde{T}^R_2} \approx \frac{4\pi}{9}\omega_Q^2\tau_s\,\ln\left(\frac{\pi N}{e}\right). \quad (7)$$

The molecular mass dependence of expression (7) is consistent with the well-known result for intramolecular proton relaxation.[30,31] The logarithmic dependence is rather weak, and thus T_2^{fast} in expression (4) can be estimated as

$$\frac{1}{\tilde{T}_2^{fast}} \sim \frac{4\pi}{9}\omega_Q^2\tau_s\,\ln\left(\frac{\pi N_e}{e}\right). \quad (8)$$

The most important factor in expression (3) that totally controls the deuteron spins HE at long times, but still $t \ll T_2^{fast}$, is the $g_{tb}^D(t)$ connected with slow reptation of polymer molecules inside the tube. The formal mathematical construction of expression (5) is identical with the initial expression (2). The difference lies in the meaning of the mathematical variables. The summation in expression (5) is carried out not over Kuhn segments, as in relation (2), but over primitive segments—$\tilde{\omega}_Q$ is the residual part of the deuteron spins quadrupole interactions after averaging over the fast local fluctuations inside the tube during times of order τ_e, $\theta_k(t_1)$ is the angle between the vector connecting the ends of the primitive segment with number k with the direction of the external magnetic field at time moment t_1, and the averaging $\langle \cdots \rangle_{rep}$ is performed over all reptation motions of the primitive chain. The residual part of the quadrupolar interaction constant $\tilde{\omega}_Q$, describing the coupling of deuteron spins with orientations of primitive segments, is related to the corresponding quadrupole coupling constant ω_Q of deuteron spins with Kuhn segment orientations, which, in usual treatment, is evaluated as $\tilde{\omega}_Q \approx \omega_Q/N_e$ (see, for example, Refs. 1 and 29). Therefore, we will introduce here a numerical factor β that depends on the specific assumptions about the configuration of the primitive path,

$$\tilde{\omega}_Q \approx \beta \frac{\omega_Q}{N_e}. \tag{9}$$

The treatment of $g_{tb}^D(t)$ is essentially different for short chains, for which the so-called Redfield limit (or the limit of fast motions) $T_2^{eff} \gg \tau_d$ holds, and for long chains in the opposite case when $T_2^{eff} \ll \tau_d$.

In the first case, the dynamic heterogeneity of linear macromolecules was considered in a recent paper[21] (some additional materials can be found in Refs. 32–36). The deuteron FID/HE of polymer chains is totally dominated by the end effects and can be expressed by the following relation:

$$g_{tb}^D(t) = \frac{1}{Z}\sum_{k=1}^{Z} \exp\left\{-\frac{6k}{Z+1}\left(1-\frac{k}{Z+1}\right)\frac{1}{\tilde{T}_2^{eff}}\right\}, \quad \text{with } \frac{1}{\tilde{T}_2^{eff}} \approx \frac{4\pi^2}{9}\tilde{\omega}_Q^2\tau_e Z^2. \tag{10}$$

Note that here we corrected the denominators inside the exponent in expression (10) in comparison to Ref. 21 by changing Z to $Z+1$. This is done because a chain containing Z segments has $Z+1$ segment ends. This difference is not important when the segment number k is considered as a continuous variable ranging from 0 to Z, as is done in the classical book,[23] but can produce artifacts in numerical calculations, when the integration over k will be implemented by a summation as in expression (10), at long times when $g_{tb}^D(t) < Z^{-1}$.

For $Z \gg 1$, the discussed expression (10) has the following asymptotic values:

$$g_{tb}^D(t) = \begin{cases} 1 - \dfrac{t}{\tilde{T}_2^{eff}} + \cdots & \text{for } t \ll \tilde{T}_2^{eff}, \\ \dfrac{\tilde{T}_2^{eff}}{3t} & \text{for } \tilde{T}_2^{eff} \ll t \ll \dfrac{Z\tilde{T}_2^{eff}}{6}, \\ \dfrac{2}{Z}\exp\left(-\dfrac{6}{Z+1}\dfrac{t}{\tilde{T}_2^{eff}}\right) & \text{for } \dfrac{Z\tilde{T}_2^{eff}}{6} \ll t. \end{cases} \tag{11}$$

The initial decay is an exponential function with the average relaxation rate $1/\tilde{T}_2^{eff} = \tilde{\omega}_Q^2\tau_e Z^2 4\pi^2/9$, followed by a drastically decreasing decay that follows a power law with exponent −1, again turning into an exponential decay at even longer times.

In the Redfield limit, the magnetizations of all subsets of spins are decaying exponentially, but spins located on different segments have different spin–spin relaxation rates. As a result, during the time interval $\tilde{T}_2^{eff} \ll t \ll Z\tilde{T}_2^{eff}/6$, the decay transforms into a power-law with exponent −1. At longer times, the decay again becomes exponential with the longest spin–spin relaxation time $T_2^{long} \cong 6\tilde{T}_2^{eff}/Z$, which has a molecular mass dependence different from that of $\tilde{T}_2^{eff}$. The Redfield limit is actually a special limit of the Anderson–Weiss approximation, which in general form for the reptation factor of the HE, i.e., $g_{tb}^D(t)$, can be described by the following expression (see, for example, Ref. 21):

$$g_{tb}^D(t) = \frac{1}{Z}\sum_{n=1}^{Z} \exp\left\{-\frac{16}{9}\frac{\tilde{\omega}_Q^2}{Z}\tau_d\sum_{p=1}^{Z}\frac{1}{p^2}\sin^2\left(\frac{\pi p n}{Z+1}\right) \times \left(t - \frac{\tau_d}{p^2}\left(1-\exp\left[-\frac{tp^2}{\tau_d}\right]\right)\right)\right\}. \tag{12}$$

Note that expressions (10) and (11) follow asymptotically from (12) in the limit $\tau_d \ll T_2^{eff}$.

For longer chains, when $T_2^{eff} \ll \tau_d$, the Redfield limit is violated and the HE decay is essentially more complex than expressions (10) and (11). The usual approach for such situations is to use the so-called Anderson–Weiss or second cumulant approximation, which, as mentioned above, is given for the reptation model by expression (12) but can be justified only for short times $t \ll T_2^{eff}$. However, as has been shown in Refs. 20 and 22, the reptation model allows us to go significantly beyond the Anderson–Weiss approximation. This is possible because the Doi–Edwards tube reptation model is based on very strong assumptions.

One of these assumptions is the postulate that during the wide range of times $\tau_e \ll t \ll \tau_d$, the polymer chains are mainly confined inside tubes and are escaping from them by one-dimensional Rouse-like motions along primitive paths. Another postulate is that the primitive path possess the conformation of an ideal chain, which corresponds to the requirement that the spatial orientation of its different primitive segments is statistically independent of each other. The latter allows us to perform averaging over the orientations of primitive segments in expression (5) independently of each other. Then, knowing that diffusion inside the tube is Rousean, by using mean field-like approximations, one can calculate the time in which the segment of the macromolecule initially localized on the kth primitive segment of the tube spent during the observation time t on the nth primitive segment of the initial tube.

The final result for $g_{tb}^{D}(t)$ caused by reptation motions inside the tube is as follows:[22]

$$g_{tb}^{D}(t) = \frac{1}{Z}\sum_{k=1}^{Z}\exp\left\{-\sum_{n=1}^{Z}\ln\left(1+\frac{2}{5}\frac{\langle\varphi_{kn}(\tilde{t}(k,t))\rangle^{2}}{1+\frac{2\pi}{5\sqrt{12}}\langle\varphi_{kn}(\tilde{t}(k,t))\rangle}\right)\right\}. \quad (13)$$

Summation over k in expression (13) is the signal contribution from the spin that, at the initial time moment $t = 0$, was located inside the primitive segment with number k of the initial tube. Summation over n inside of the exponents in expression (13) reflects the one-dimensional Rousean displacements of it inside the initial tube. With an increase in the observation time t, the polymer segments change their positions inside the initial tube and can be located in the position where the primitive segment with number n was located initially. Generally speaking, the segment with number k does not spend the complete observation time t inside the initial tube since it can exit from it. We call $\tilde{t}(k,t)$ the period that segment k spends inside the tube during t, so that it has spent $t - \tilde{t}(k,t)$ outside of it. For $\tilde{t}(k,t)$, one can make the following approximation[22] for times $t \ll \tau_d$:

$$\tilde{t}(k,t) = \frac{t}{1+\sqrt{\frac{9\pi}{32}}\tilde{n}(t)\left(\frac{1}{k}+\frac{1}{Z+1-k}\right)}, \quad (14)$$

where $\tilde{n}(t) = \langle s^2(t)\rangle^{1/2}/a$ is the characteristic number of primitive segments on which polymer segments are displaced inside the tube during time interval t and $\langle s^2(t)\rangle$ is the mean squared displacement of polymer segments inside the tube, which can be approximated by relation (1).

The quantity $\langle\varphi_{kn}(\tilde{t}(k,t))\rangle$ is defined by the following relation:[22]

$$\langle\varphi_{kn}(\tilde{t}(k,t))\rangle = \tilde{\omega}_Q\int_0^{\tilde{t}(k,t)}dt_1\sqrt{\frac{a^2}{2\pi\langle s^2(t_1)\rangle}}\left[\exp\left\{-\frac{1}{2}\frac{(n-k)^2a^2}{\langle s^2(t_1)\rangle}\right\} - \exp\left\{-\frac{1}{2}\frac{(n+k)^2a^2}{\langle s^2(t_1)\rangle}\left(1-\frac{n+k}{2(Z+1)}\right)^2\right\}\right]. \quad (15)$$

As has been discussed above, in comparison to expression (32) in Ref. 22, Z has been replaced by $Z + 1$ in the second exponent. The second term inside the integral depending on the sum of the numbers $n + k$ of primitive segments, i.e., on the position relative to the ends of the polymer chain, describes the dynamical heterogeneity of the polymer chain arising from end segments. As time increases, this contribution increases as well, since an increasing number of segments can be considered as end segments; in other words, the effect of end segments has a frequency nature, i.e., depends on observation time.

The expressions (1), (3), and (13)–(15) allow a closed description of the HE of reptating chains for long time interval $\tau_e \ll t \ll \tau_d$ in terms of $\tilde{\omega}_Q$, Z, τ_e, and a. For qualitative comparison, some analytical asymptotic expressions following from expression (13) are of interest:[22]

The initial ($\tau_e \ll t \ll T_2^{eff}$) behavior of the HE depends on the relationships between the effective spin–spin relaxation time T_2^{eff} and the characteristic relaxation times of the tube-reptation model τ_e, τ_R, and τ_d. If the polymer chains are long enough, then, at temperatures typical for melts, the relation $\tau_e \ll T_2^{eff} \ll \tau_R$ is valid. For this case, the deuteron HE reflects motions of polymers in the region of *incoherent* reptation, i.e., in region II. The initial HE will be a pseudo-Gaussian with exponent 7/4,

$$g_{tb}^{D}(t) = 1 - \left(\frac{t}{\tilde{T}_2^{eff}}\right)^{7/4} + \cdots, \quad (16)$$

with an effective spin relaxation time

$$\tilde{T}_2^{eff} = \left(\frac{105}{32\sqrt{3\pi^{1/2}}\left(2-\sqrt{2}\right)}\right)^{4/7}\frac{1}{\tilde{\omega}_Q(\tilde{\omega}_Q\tau_e)^{1/7}} \approx \frac{1.66}{\tilde{\omega}_Q(\tilde{\omega}_Q\tau_e)^{1/7}}. \quad (17)$$

For shorter chains satisfying the relation $\tau_R \ll T_2^{eff} \ll \tau_d$, the HE reflects motions of the polymer chains in the region of *coherent* reptation, i.e., in region III. The initial time dependence of the HE is again pseudo-Gaussian, but with an exponent 3/2,

$$g_{tb}^{D}(t) = 1 - \left(\frac{t}{\tilde{T}_2^{eff}}\right)^{3/2} + \cdots, \quad (18)$$

with the effective spin-relaxation time

$$\tilde{T}_2^{eff} = \left(\frac{5}{4}\sqrt{\frac{3}{4\pi}}\right)^{2/3}\frac{1}{\tilde{\omega}_Q(\tilde{\omega}_Q\tau_e)^{1/3}Z^{1/3}} \approx \frac{0.72}{\tilde{\omega}_Q(\tilde{\omega}_Q\tau_e)^{1/3}Z^{1/3}}. \quad (19)$$

At longer times $T_2^{eff} \ll t \ll \tau_d$, the time dependence of $g_{tb}^{D}(t)$—within an accuracy of logarithmic corrections—becomes a stretched exponential with the detailed properties differing between the regions of incoherent and coherent reptation. In the region of incoherent reptation, when $\tau_e < t < \tau_R$, the decay of $g_{tb}^{D}(t)$ can be approximated by the following expression:

$$g_{tb}^{D}(t) \approx \left(1-\sqrt{\frac{8}{3\pi^{3/2}Z^2}}\left(\frac{t}{\tau_e}\right)^{1/4}\right) \times \exp\left\{-\sqrt{\frac{8}{3\pi^{3/2}}}\left(\frac{t}{\tau_e}\right)^{1/4}\ln\left(\frac{16}{\sqrt{2\pi^{3/2}}}\tilde{\omega}_Q t^{3/4}\tau_e^{1/4}\right)\right\} + \frac{8}{Z}\frac{\exp\left\{-\left(\frac{2}{3\pi^{3/2}}\right)^{3/8}\left(\frac{t}{\tau_e}\right)^{3/16}\ln\left(\frac{16}{\pi^{5/8}}\frac{3^{3/4}}{e}\tilde{\omega}_Q t^{5/8}\tau_e^{3/8}\right)\right\}}{\left(\frac{2}{3\pi^{3/2}}\right)^{3/8}\left(\frac{t}{\tau_e}\right)^{3/16}\ln\left(\frac{16}{\pi^{5/8}}\frac{3^{3/4}}{e}\tilde{\omega}_Q t^{5/8}\tau_e^{3/8}\right)}. \quad (20)$$

On the other hand, in the region of coherent reptation, when $\tau_R < t < \tau_d$, the decay of $g_{tb}^{D}(t)$ can be described as

$$g_{tb}^{D}(t) \approx \left(1-\sqrt{\frac{8}{3\pi^2Z^2}}\left(\frac{t}{Z\tau_e}\right)^{1/2}\right) \times \exp\left\{-\sqrt{\frac{8}{3\pi^2}}\left(\frac{t}{Z\tau_e}\right)^{1/2}\ln\left(\sqrt{\frac{6}{\pi}}\tilde{\omega}_Q t^{1/2}\tau_e^{1/2}Z^{1/2}\right)\right\} + \frac{1}{Z}\frac{\exp\left\{-\left(\frac{16t}{3\pi^3Z\tau_e}\right)^{1/4}\ln\left(\frac{2^{5/2}3^{9/4}}{e\sqrt{\pi}}\tilde{\omega}_Q t^{1/4}\tau_e^{3/4}Z^{1/4}\right)\right\}}{\left(\frac{16t}{3\pi^3Z\tau_e}\right)^{1/4}\ln\left(\frac{2^{5/2}3^{9/4}}{e\sqrt{\pi}}\tilde{\omega}_Q t^{1/4}\tau_e^{3/4}Z^{1/4}\right)}. \quad (21)$$

The first terms on the right-hand side of expressions (20) and (21) are connected with central segments, and the second terms represent the end effects.

III. METHODS

For the experimental part of this study, perdeuterated polyethylene oxide of different molar masses (see Table I) was purchased from Polymer Standards Service GmbH, Mainz, Germany. The PEO samples were placed in 3 mm outer diameter NMR tubes, covered with argon, and flame sealed. The transverse relaxation decay of the deuterons was measured with a Bruker Avance III NMR spectrometer operating at a ^{2}H resonance frequency of 46.1 MHz equipped with a solid state probe head, using a Hahn echo pulse sequence $(90^\circ_x - \tau - 180^\circ_x - \tau)$ with appropriate phase cycling. The duration of the π-pulse, typically 10 μs, was twice the length of the $\pi/2$-pulse. The measurements were carried out in completely molten state of the polymers at different temperatures between the melting point (see Table I) and 373 K. The longitudinal relaxation time T_1 increases for all samples with temperature, i.e., from roughly 40 ms (T_m) to about 100 ms (373 K). A recycle delay of 5 T_1 was applied between the repetitions of the pulse sequence to allow for a complete spin–lattice relaxation. Starting from the end of the second waiting time τ, the second half of the spin-echo was acquired. The transverse relaxation decay is then given by the evolution of the PEO echo intensity at time $t = 2\tau + t_\pi$. The measurements were repeated up to five times, normalized to their maximum, and then averaged (for details, see Ref. 37).

IV. RESULTS AND DISCUSSION

In the following, the relevant time scales (τ_s, τ_e, τ_R, and τ_d) are estimated, before the experimental results are being discussed in the context of the presented theory. The segmental relaxation time can be estimated by using the entanglement molecular mass M_e = 1730 g/mol,[38] the center of mass diffusion for the reference molecular weight $D_{cm}(12.3\text{k}) = 3 \times 10^{-13}\text{m}^2/s$,[39] the Kuhn length b = 11Å, and the molecular mass of a Kuhn segment m_k = 137 g/mol[25] as follows:

$$\tau_s = \frac{1}{9\pi^2}\frac{b^2 N_e}{D_{\text{cm}} N_{\text{cm}}^2} \cong 7.1 \times 10^{-11}\text{s}, \tag{22}$$

with $N_e = M_e/m_k \cong 12.6$ and $N_{cm} = M_{cm}/m_k \cong 89.8$. Correspondingly, the entanglement time is estimated as follows:

$$\tau_e = \tau_s N_e^2 \cong 1.1 \times 10^{-8}\text{s}. \tag{23}$$

From this, we can now estimate the Rouse relaxation and tube disengagement times for the investigated molecular weights according to $\tau_R = \tau_s N^2 = \tau_e Z^2$ and $\tau_d = 3\tau_e Z^3$.

By comparing τ_d with T_2^{eff} in Table II, it is obvious that the samples PEO-d_4 3.5k and PEO-d_4 33k satisfy the conditions of the Redfield limit $\left(T_2^{eff} \gg \tau_d\right)$, while PEO-$d_4$ 75k is in the crossover region $\left(T_2^{eff} \approx \tau_d\right)$, and the sample with the largest molecular mass PEO-d_4 300k is beyond the Redfield limit $\left(T_2^{eff} \ll \tau_d\right)$. For this molecular mass, the Rouse relaxation time is in the order of T_2^{eff}, and therefore most of the experimental time scale lies in the region of coherent reptation, i.e., in region III, as one can see on the left side of Fig. 1. In contrast, for the samples with a lower molecular mass, $T_2^{eff} \gtrsim \tau_d$ so that most of the experimental time scale lies in region IV.

From expression (7), consequently, the temperature dependence of T_2^{eff} is determined by the temperature dependence of the segmental relaxation time τ_s^{-1}, which also defines the temperature dependence of the self-diffusion coefficient. In the regions of incoherent and coherent reptation, the temperature dependence of T_2^{eff} is expected to be weaker, following $\tau_s^{-1/7}$ and $\tau_s^{-1/3}$, as can be seen in expressions (17) and (19), respectively.

Indeed, the experimental results seem to support these assumptions, as can be seen in Fig. 1(b) and Table III. The activation energies obtained from T_2^{eff} for the three lowest molecular masses (3.5k, 33k, and 75k) are close to each other and in agreement with results of rheological measurements $[E_a(10\text{k})/k_B = 3020\text{ K}]$.[40] For the largest molecular mass (300k), the effective activation energy is significantly smaller. At least in a semi-quantitatively approach, this is in accordance with tube-reptation predictions for region III, i.e., coherent reptation.

In the following, the theoretical predictions of the Hahn echo decays will be compared to the experimental results at 358 K, since the shape of the decay remains unchanged in the investigated temperature regime and the used literature values are mainly valid for

TABLE I. Sample overview. Samples, as well as molecular weight and polydispersity index data, were provided by Polymer Standards Service GmbH, Mainz, Germany. The melting temperatures T_m were determined by dynamic scanning calorimetry using a Perkin Elmer DSC 6000 instrument. The specified melting temperatures correspond to the peak temperature in the second heating run at 1 K/min (for details, see Ref. 37).

	T_m (°C)	M_w (g/mol)	M_p (g/mol)	M_n (g/mol)	PDI
PEO-d_4 300k	56.0	310 000	289 000	242 000	1.28
PEO-d_4 75k	57.6	74 100	79 500	61 000	1.21
PEO-d_4 33k	55.7	34 400	34 700	31 300	1.10
PEO-d_4 3.5k	48.4	3 410	3 600	3 080	1.11

TABLE II. Number of entanglements per chain, Rouse relaxation time, and tube disengagement time of our samples based on the number average molecular mass M_n. The comparison of τ_d with the experimental T_2^{eff} shows the validity of the Redfield limit for the corresponding sample. Since the literature values in Refs. 38 and 39, and thus the calculated times, are given for 353 K, we show our results for 358 K to ensure the maximum possible comparability.

	Z	τ_R (s)	τ_d (s)	T_2^{eff} (358 K) (s)
PEO-d_4 300k	140	2.2×10^{-4}	9.3×10^{-2}	8.8×10^{-4}
PEO-d_4 75k	35	1.4×10^{-5}	1.5×10^{-3}	2.2×10^{-3}
PEO-d_4 33k	18	3.7×10^{-6}	2.0×10^{-4}	7.0×10^{-3}
PEO-d_4 3.5k	2	4.5×10^{-8}	2.7×10^{-7}	5.6×10^{-2}

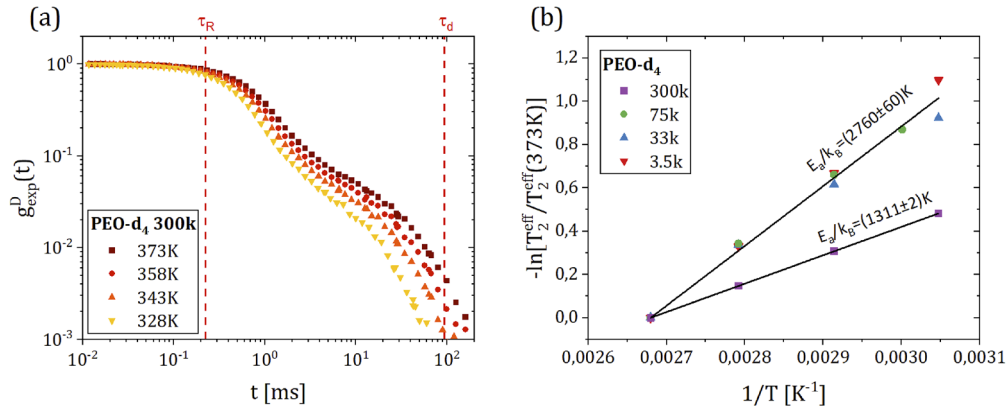

FIG. 1. (a) Hahn echo decay for PEO-d4 300k at four temperatures between 328 K and 378 K. Most of the investigated time scale lies between the estimated τ_R and τ_d (dashed lines), i.e., within region III. The experimental T_2^{eff} increases with temperature, while the shape of the decay remains unchanged. (b) Temperature dependence of T_2^{eff} in form of the negative logarithm of T_2^{eff} normalized to 373 K over the inverse temperature. In this representation, the activation energy E_a/k_B results directly from the slope of the regression line. A significant difference is observed between 300k and the other molar masses. The activation energy for each sample is listed in Table III.

353 K, assuming that the reptation model without the effects of contour length fluctuations adequately describes the real chain motions in polymer melts. Let us first investigate the ^{2}H NMR response considering the lowest molecular masses of 3.5k and 33k. Both situations are within the validity of the Redfield limit. The measured spin–spin relaxation rates can be represented as the sum of contributions from the fast fluctuating Rouse modes inside the tube and slow fluctuating reptation modes connected with diffusion inside tubes,

$$R_2(M_i) = R_2^{Rep}(M_i) + R_2^{Rouse}(M_i) = \frac{1}{T_2^{Rep}(M_i)} + \frac{1}{T_2^{Rouse}(M_i)}, \quad (24)$$

where R_2 are the experimentally measured effective spin–spin relaxation rates of samples with the molecular weights M_i. The Rouse relaxation time depends only weakly on the molecular mass [see expression (6)], and therefore, it seems reasonable to accept as a first estimation $R_2^{Rouse}(M_1) = R_2^{Rouse}(M_2)$. The contributions of reptation modes can be estimated using expression (10), where the values of two different molecular masses are related as follows:

$$\frac{R_2^{Rep}(M_2)}{R_2^{Rep}(M_1)} = \left(\frac{Z_2}{Z_1}\right)^2. \quad (25)$$

Using expressions (24) and (25) in combination with the experimentally measured values for M_1 = 3.5k and M_2 = 33k at 358K (see Tables II and III), we can estimate the reptation contribution for PEO-d$_4$ 3.5k as

$$R_2^{Rep}(M_1) = \frac{R_2(M_2) - R_2(M_1)}{\left(\frac{Z_2}{Z_1}\right)^2 - 1} \approx 0.098 R_2(M_1). \quad (26)$$

Thus, the HE decay of 3.5k is dominated by the Rouse modes (90.2%). We can now estimate β^2 by dividing expression (7) by expression (10),

$$\beta^2 = \frac{R_2^{Rep}(M_2)}{R_2^{Rouse}(M_1)} \frac{\ln\left(\frac{\pi N_1}{e}\right)}{\pi Z_2^2} = \frac{R_2(M_2) - R_2^{Rouse}(M_1)}{R_2^{Rouse}(M_1)} \frac{\ln\left(\frac{\pi N_1}{e}\right)}{\pi Z_2^2}. \quad (27)$$

Using $R_2^{Rouse}(M_1) = 0.902 R_2(M_1)$ and $N_1 = M_n(3.5\text{k})/m_k$, one finds $\beta^2 \approx 1/40$.

One possible explanation for this rather small value of β may be related to the primitive chain conformation. It is very well known that long-wavelength properties of sufficiently long ideal chains are equivalent to each other.[23–27] This means that it is irrespective of the model, i.e., freely jointed chain of Kuhn, Gaussian chain, worm-like chain (persistent chain or Kratky–Porod chain[41]), or some other is being used for describing them. However, the situation may turn out to be different if one addresses short-wavelength properties that depend on the structure of the chain segment. The discussed parameter β connected with the residual part of quadrupole interactions of deuterium spins [see expression (9)] seems to belong to these short-wavelength properties.

TABLE III. Experimental effective spin–spin relaxation time T_2^{eff}, i.e., the time needed for the signal to decay from the initial normalization 1 to 1/*e* and resulting activation energies E_a/k_B.

	PEO-d$_4$ 300k	PEO-d$_4$ 75k	PEO-d$_4$ 33k	PEO-d$_4$ 3.5k
T_2^{eff} (373 K)(s)	1.02×10^{-3}	3.1×10^{-3}	9.8×10^{-3}	7.8×10^{-2}
T_2^{eff} (358 K)(s)	8.8×10^{-4}	2.2×10^{-3}	7.0×10^{-3}	5.6×10^{-2}
T_2^{eff} (343 K)(s)	7.5×10^{-4}	1.6×10^{-3}	5.3×10^{-3}	4.0×10^{-2}
T_2^{eff} (333 K)(s)		1.3×10^{-3}		
T_2^{eff} (328 K)(s)	6.3×10^{-4}		3.9×10^{-3}	2.6×10^{-2}
E_a/k_B (K)	1311 ± 2	2700 ± 100	2480 ± 120	2970 ± 70

In the standard formulation of the tube-reptation model,[23–27] the primitive path and the primitive chain are considered either as a freely jointed chain consisting of Z Kuhn segments of length $a = bN_e^{1/2}$ or as a Gaussian chain for discussing the effects connected with contour length fluctuations. The primitive path is, by definition, the line around which the fast Rouse-like motions of polymer segments are being performed at a distance about the tube diameter $a = bN_e^{1/2}$. This constitutes a very complex dynamical object of intermolecular entanglements formed during a time interval $\tau_e = \tau_s N_e^2$. Therefore, it seems more realistic to consider it as a continuous line slowly changing in direction. The worm-like ideal chain (or persistent, Kratky–Porod chain[24,41,42]) should be more realistic for a description of the primitive path.

For the worm-like chains, as it is very well known,[24,41,42] the square of the Flory radius $\langle R_F^2 \rangle$ is connected with the persistent chain length l_p and the extended length of the chain L by the following relation:

$$\langle R_F^2 \rangle = 2Ll_p - 2l_p^2\left(1 - \exp\left\{-\frac{L}{l_p}\right\}\right). \tag{28}$$

From this relation, consequently, the length of the Kuhn segment for the worm-like chain equals

$$b_p \equiv \frac{\langle R_F^2 \rangle}{L} = 2l_p - \frac{2l_p^2}{L}\left(1 - \exp\left\{-\frac{L}{l_p}\right\}\right). \tag{29}$$

If the length of the worm-like chain is large, $L \gg l_p$, then the Kuhn segment is connected by simple relation with the persistence length as follows:

$$b_p \cong 2l_p. \tag{30}$$

However, there exists an important difference between the freely jointed chain with Kuhn segments of length b_p and the worm-like chain with the same length of the Kuhn segment. A freely jointed chain consists of rectilinear segments with length $b_p = 2l_p$, while the worm-like chain is curved on each of its points. As a result, the length of the Kuhn segment in space and along the segment are identical, while the Kuhn segment in the case of the worm-like chain is an effective quantity where the separation of the segment in space and along the segment differs (see Fig. 2). If we consider two points of a worm-like chain separated in space by the distance $b_p = 2l_p$, the separation of the points along the chain s in comparison with the freely jointed chain and in accordance with relation (28) would satisfy the following equation:

$$b_p s^{fj} = 4l_p^2 = 2s^{wl}l_p - 2l_p^2\left(1 - \exp\left\{-\frac{s^{wl}}{l_p}\right\}\right). \tag{31}$$

This transcendental equation can be solved numerically with respect to s^{wl} and results in $s^{wl} \cong 2.9475l_p \approx 3l_p$. For two points inside the worm-like chain at positions x_1 and x_2, the corresponding tangent vectors $\vec{u}(x_1)$ and $\vec{u}(x_2)$ are not parallel to each other (see Fig. 2), and the average cosine of the angle between them can be calculated in the following way:

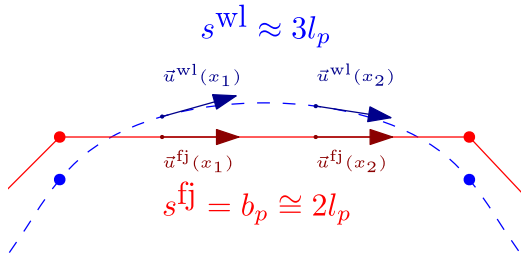

FIG. 2. Illustration of the differences between the worm-like (wl, dashed line) and freely jointed (fj, solid line) chains regarding the length of the Kuhn segment for two points separated in space by $b_p = 2l_p$ and the orientation of the tangent vectors $\vec{u}_1(x_1)$ and $\vec{u}_2(x_2)$ at two positions x_1 and x_2, respectively.

$$\begin{aligned}\langle \cos\theta_{12} \rangle &= \frac{1}{\tilde{s}^2}\int_0^{\tilde{s}} dx_1 \int_0^{\tilde{s}} dx_2 \langle \vec{u}(x_1) \cdot \vec{u}(x_2) \rangle \\ &= \frac{1}{\tilde{s}^2}\int_0^{\tilde{s}} dx_1 \int_0^{\tilde{s}} dx_2 \, \exp\left\{-\frac{|x_1 - x_2|}{l_p}\right\} \\ &= \frac{2l_p}{\tilde{s}}\left(1 - \frac{l_p}{\tilde{s}} + \frac{l_p}{\tilde{s}}\exp\left\{-\frac{\tilde{s}}{l_p}\right\}\right) \approx 0.460. \end{aligned} \tag{32}$$

Let us assume a case where the primitive path is the freely jointed chain consisting of $Z = N/N_e$ Kuhn segments, where N is the number of segments inside the real tagged polymer chain and N_e is the number of Kuhn segments between two entanglements. The vectors connecting the ends of the primitive segments are denoted as $\vec{a}_k$ with $k = 1, 2, \ldots, Z$. Consider a situation when the segment of the tagged chain with number m is located somewhere in the vicinity of the primitive segment with number k. In this case, a residual part of the projection of the vector connecting the ends of the mth segment of the tagged chain on the vector $\vec{a}_k$ does not depend on the position inside the kth primitive segment where it is located because the latter is a straight line. The situation is different for the case when the primitive path has the structure of a worm-like chain because its segments are curved. Therefore, this situation will lead to the appearance of an additional numerical factor given by expression (32). The Hamiltonian of deuteron quadrupole interactions depends quadratically with respect to the relative variables connected with segment orientation (it is an irreducible tensor of the second order relatively angle variables of the Kuhn segment), and therefore expression (9) can be rewritten as

$$\tilde{\omega}_Q = \beta\frac{\omega_Q}{N_e} = \tilde{\beta}\langle \cos\theta_{12} \rangle^2 \frac{\omega_Q}{N_e}, \tag{33}$$

where the numerical factor $\tilde{\beta}$ is retained to account for possible additional factors.

The effective spin relaxation rate, as it is possible to see from expression (10) in the Redfield limit, is proportional to $\tilde{\omega}_Q^2 = \tilde{\beta}^2\langle \cos\theta_{12} \rangle^4 \omega_Q^2 N_e^{-2}$, where $\langle \cos\theta_{12} \rangle^4 \approx 1/22$ is comparable to the value estimated from the experimental data $\beta^2 \approx 1/40$.

In the following, we attempt a comparison between the experimentally observed HE decays of deuterated PEO melts (3.5k, 33k, 75k, and 300k) and the decays predicted by the discussed theory using expressions (1)–(15) for an extended time interval $t \leq 10T_2^{eff}$, as presented in Figs. 3–7.

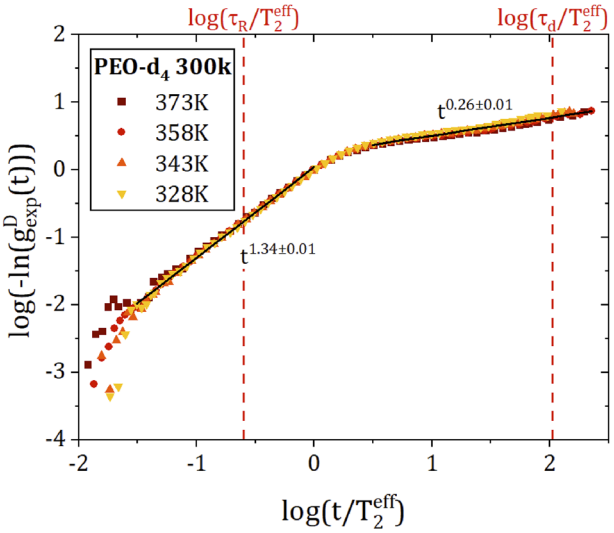

FIG. 3. Double logarithm of the normalized Hahn echo signal $\log\left(-\ln\left(g^D_{exp}(t)\right)\right)$ as a function of the logarithm of the normalized time $\log\left(t/T_2^{eff}\right)$. The slopes of the linear fit (solid lines) in the short- and long-time regions yield the exponents of the pseudo-Gaussian and stretched exponential decays. The estimated Rouse and tube disengagement times corresponding to 358 K are marked with dashed lines.

One can see a qualitative correspondence between the predictions of the reptation model and the experimentally observed ^{2}H HE decay, consisting of a strong attenuation of the initial decay at times exceeding T_2^{eff}. This attenuation reflects both the frequency nature

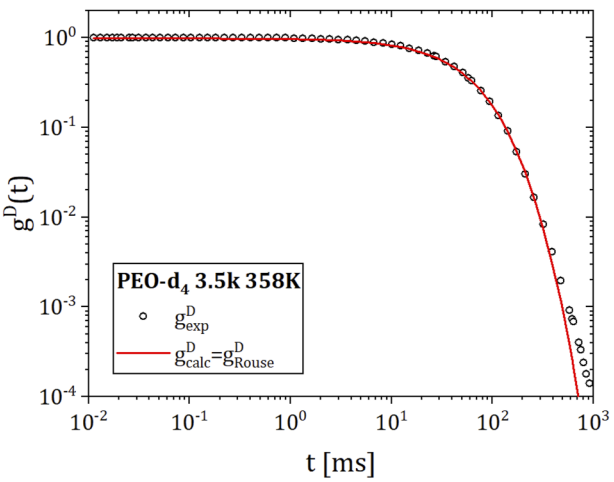

FIG. 4. Deuteron Hahn echo decay of PEO-d_4 3.5k at 358K (circles) in comparison with the calculated decay for non-entangled polymer melts (line) according to expression (6) using the corresponding numbers from Table II and ω_Q = 230 000 s^{-1}. Note that the Rouse relaxation time $\tau_R \approx 4.5 \times 10^{-8}$ s and the tube disengagement time $\tau_d \approx 2.7 \times 10^{-7}$ s for this molar mass are essentially smaller than the presented time window.

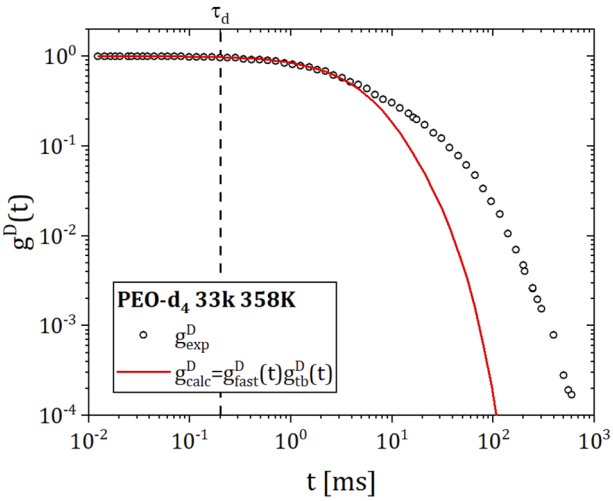

FIG. 5. Deuteron Hahn echo decay of PEO-d_4 33k at 358K (circles) in comparison with the calculated decay for entangled polymers inside the Redfield limit (line) according to expression (3) with expression (4) for g^D_{fast} and expression (12) for g^D_{tb}. T_2^{fast} would be ideally determined in a sample with $M < M_e$; however, the sample 3.5k is close to the limit of entanglements ($M \approx 2M_e$) and can, therefore, be used as lower limit for T_2^{fast}, so that $T_2^{fast} = T_2^{eff}(3.5\text{k}) = 56$ ms. For g^D_{tb}, the corresponding numbers from Table II were used with $\tilde{\omega}_Q = 3300\ s^{-1}$. The estimated tube disengagement time is depicted by the dashed line. Note that the Rouse relaxation time $\tau_R \approx 3.7 \times 10^{-6}$ s for this molecular mass is essentially smaller than the presented time window.

of the end effect and the reptation movements of the polymer chains within the tubes created by entanglements.

This qualitative agreement is displayed in Fig. 3, which shows the time dependence of the Hahn echo signal measured in units of the experimentally determined effective spin relaxation time T_2^{eff} in double logarithmic coordinates for the PEO-d_4 300k melt at different temperatures. The time interval under discussion corresponds to the coherent reptation region, i.e., regime III. Experimentally, we observe a transition from a pseudo-Gaussian decay at short times with an effective exponent of 1.34 to a stretched exponential decay with an exponent of 0.26. This compares to a transition from pseudo-Gaussian behavior given by expression (18) with the exponent 1.5 at short times to the nearly (i.e., with accuracy of logarithmic corrections) stretched exponential decay given by expression (21) at longer times. The observed stretched exponent 0.26 corresponds to the second term in the right-hand side of expression (21) reflecting the frequency nature of the end effects.

As already mentioned, PEO-d_4 3.5k and 33k satisfy the Redfield limit, 75k is in the crossover region, and 300k is beyond the Redfield limit. Furthermore, 3.5k has a molecular mass of about twice M_e. Therefore, for quantitative comparison, we attempt to describe 3.5k with expression (6), 33k and 75k with expression (12), and 300k with expression (13) in combination with expressions (1), (14), and (15).

In Fig. 4, one can see the Hahn echo decay of the PEO-d_4 3.5k melt. Despite the fact that the discussed molecular weight is approximately twice as large as N_e and we are dealing at least with a weakly meshed melt, the echo signal decay is well described by expression (6), derived for the Rouse model taking into account

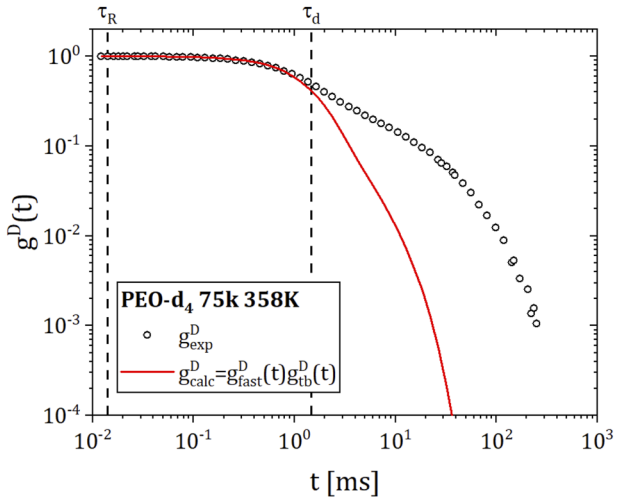

FIG. 6. Deuteron Hahn echo decay of PEO-d_4 75k at 358K (circles) in comparison with the calculated decay for entangled polymers inside the Redfield limit (line) according to expression (3) with expression (4) for g^D_{fast} and expression (12) for g^D_{tb}, using T_2^{fast} = 56 ms, $\tilde{\omega}_Q$ = 4200 s^{-1}, and the values from Table II. The estimated Rouse and tube disengagement times are depicted by dashed lines.

the dynamical heterogeneity of polymer segments connected with the end-effects. This is in agreement with the previously estimated contributions of 90.2% Rouse and 9.8% reptation modes.

In Figs. 5–7, we present our attempts to match the experimentally observed HE decays for PEO-d_4 33k, 75k, and 300k at 358K with the decays described by expressions (1) and (12)–(15) derived from the tube-reptation model. One can see that a more or less satisfactory description is achieved only in the initial part of the attenuation. At longer times, the tube-reptation model predicts a faster decay than is actually observed experimentally. This reflects an overestimation by the tube-reptation model of anisotropic reptation modes, i.e., by strong correlations of segment spatial displacements with the initial polymer chain conformation, and a corresponding underestimation of isotropic fluctuations of the remaining modes of motion, as is postulated by the Renormalized Rouse models (see details in review articles[2,6,43]).

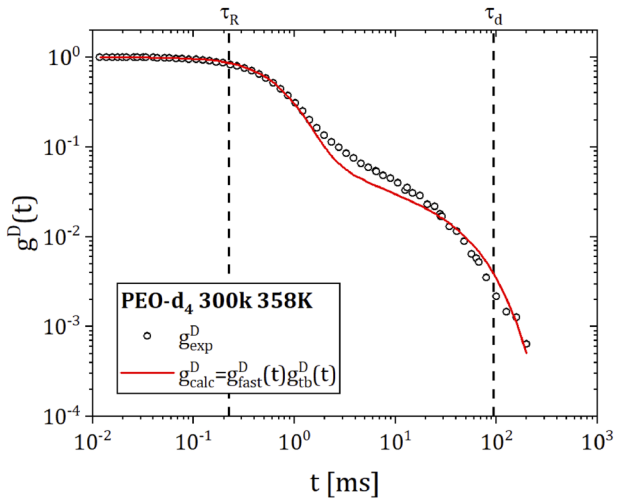

FIG. 7. Deuteron Hahn echo decay of PEO-d_4 300k at 358K (circles) in comparison with the calculated decay for entangled polymers outside the Redfield limit (line) according to expression (3) with expression (4) for g^D_{fast} and expression (13) in combination with expressions (1), (14), and (15) for g^D_{tb}, using T_2^{fast} = 56 ms, $\tilde{\omega}_Q$ = 11 200 s^{-1}, and the values from Table II. The estimated Rouse and tube disengagement times are depicted by dashed lines.

This can also be seen in Fig. 8, where the experimentally observed molecular mass dependence of T_2^{eff} is illustrated. A nearly linear dependence on molecular mass $1/T_2^{eff} \sim Z = N/N_e$ is observed, while from expression (10), a quadratic dependence $1/\tilde{T}_2^{eff} \sim Z^2$ is expected for situations where the Redfield limit is met and a dependence of $1/\tilde{T}_2^{eff} \sim Z^{1/3}$ for situations outside that limit, according to expression (19).

Here, however, the difference between $\tilde{T}_2^{eff}$ and T_2^{eff} needs to be noted. The first one is defined by expression (10), which is actually the initial decay rate of the HE. The second one is defined by the equation $g^D\left(T_2^{eff}\right) = 1/e$. In our cases, when the conditions of the Redfield limit are satisfied, this equation can be read as

$$g^D\left(T_2^{eff}\right) = \frac{1}{Z}\sum_{k=1}^{Z} \exp\left\{-\frac{6k}{Z+1}\left(1-\frac{k}{Z+1}\right)\frac{T_2^{eff}}{\tilde{T}_2^{eff}}\right\} = \frac{1}{e}. \quad (34)$$

In the limit $Z \to \infty$, the equality $T_2^{eff} = \tilde{T}_2^{eff}$ will hold; however, for small Z, both quantities will have a different dependence on molecular mass. The described situation can partially be mitigated by a small value of the numerical factor β in expression (9). To our knowledge, this point has not yet been investigated necessarily but could at least partially explain the aforementioned discrepancy in the future.

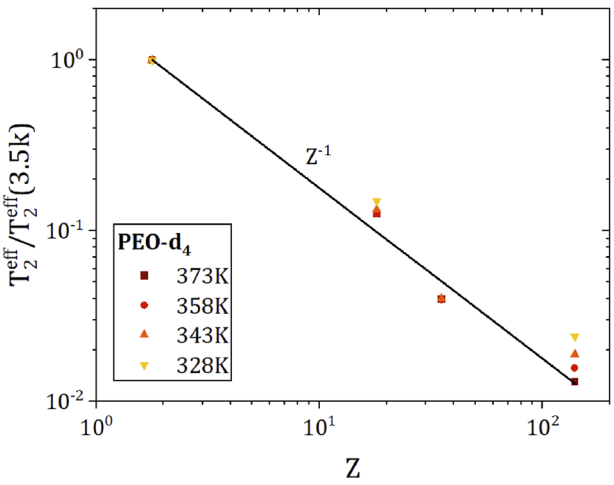

FIG. 8. Dependence of the normalized experimental T_2^{eff} on $Z = M_n/M_e$. For comparison, a dependence on Z^{-1} is shown as solid line.

In this paper, we have focused on the detailed discussion of the most popular dynamic model of reptations, which is phenomenological in nature. In addition, there are microscopic approaches based on the Zwanzig-Mori memory matrix formalism developed initially in the works of Schweizer[44–46] and extended by Kimmich and Fatkullin as a variant related to the renormalized Rouse formalism.[2,47–50] This approach is based on the pre-averaging approximation in the derivation of the equations of motion of the polymer chain, which absolutely exclude anisotropic reptation motions along the primitive tube. The preliminary calculations based on the thrice renormalized Rouse model show better agreement with our experimental results for the molar masses up to 75k, for which the Anderson–Weiss approximation can be used. Further theoretical and experimental research, and mutual comparison are required to improve the understanding of long-chain polymer dynamics.

V. CONCLUSIONS

The phenomenological tube-reptation model is formulated for the limit of infinitely long polymer chains. In melts of macromolecules for experimentally accessible finite molecular masses, contributions from non-reptational modes of motion to experimentally observed physical quantities, whose behavior differs significantly from the predictions of the reptation model, turn out to be important. Systematic studies of the dynamics of the spin echo signal decay of deuterium nuclei in polymer melts of various molecular masses over long time intervals, significantly longer than the effective spin–spin relaxation time, and comparison with corresponding decays from proton spins in undeuterated polymer melts, contains unique and new information on the molecular mechanisms of the intermolecular entanglement formation process. In our opinion, this is still a poorly understood fundamental process of entanglement formation that can be investigated by thorough NMR transverse relaxation studies in polymer melts with molecular masses of 50–100 kDa, for which the Anderson–Weiss approximation should be correct, and will make the interpretation of the experimental data more reliable in order to allow for refinements of the current reptation models.

ACKNOWLEDGMENTS

The authors acknowledge financial support from the Deutsche Forschungsgemeinschaft under research Grant No. STA 511/13-2. They also acknowledge financial support for the publication from the Open Access Publication Fund of the Technische Universität Ilmenau. The authors thank Kerstin Geyer for assistance with the DSC measurements.

AUTHOR DECLARATIONS

Conflict of Interest

The authors have no conflicts to disclose.

Author Contributions

K. Lindt: Data curation (lead); Formal analysis (lead); Investigation (lead); Software (lead); Visualization (lead); Writing – review & editing (equal). **C. Mattea:** Software (supporting); Supervision (equal); Writing – review & editing (equal). **S. Stapf:** Conceptualization (equal); Funding acquisition (lead); Methodology (supporting); Project administration (lead); Resources (lead); Supervision (equal); Writing – review & editing (equal). **I. K. Ostrovskaya:** Software (supporting); Writing – review & editing (equal). **N. F. Fatkullin:** Conceptualization (equal); Methodology (lead); Supervision (equal); Writing – original draft (lead).

DATA AVAILABILITY

The data that support the findings of this study are openly available in Figshare at http://doi.org/10.6084/m9.figshare.19762933, reference number [37].

REFERENCES

[1] J. P. Cohen-Addad, Prog. Nucl. Magn. Reson. Spectrosc. **25**, 1 (1993).
[2] R. Kimmich and N. Fatkullin, Adv. Polym. Sci. **170**, 1 (2004).
[3] K. Saalwächter, Prog. Nucl. Magn. Reson. Spectrosc. **51**, 1 (2007).
[4] J. Kowalewski, *Nuclear Magnetic Resonance* (RSC Publishing, 2011), Vol. 40, p. 205.
[5] D. Kruk, A. Herrmann, and E. A. Rössler, Prog. Nucl. Magn. Reson. Spectrosc. **63**, 33 (2012).
[6] R. Kimmich and N. Fatkullin, Prog. Nucl. Magn. Reson. Spectrosc. **101**, 18 (2017).
[7] J. P. Cohen-Addad, J. Chem. Phys. **60**, 2440 (1974).
[8] V. D. Fedotov, V. M. Chernov, and T. N. Khazanovich, Polym. Sci. U.S.S.R. **20**, 1037 (1978).
[9] J. P. Cohen-Addad and R. Dupeyre, Polymer **24**, 400 (1983).
[10] T. P. Kulagina, V. V. Marchenkov, and B. N. Provotorov, Polym. Sci. U.S.S.R. **31**, 420 (1989).
[11] M. G. Brereton, Macromolecules **22**, 3667 (1989).
[12] M. G. Brereton, Macromolecules **23**, 1119 (1990).
[13] V. M. Chernov and G. S. Krasnopol'skii, J. Exp. Theor. Phys. **107**, 302 (2008).
[14] V. M. Chernov and A. V. Butakov, Polym. Sci., Ser. A **53**, 204 (2011).
[15] C. P. Slichter, *Principles of Magnetic Resonance*, 3rd ed. (Springer, Berlin, 1992).
[16] D. Wolf, *Spin-Temperature and Nuclear-Spin Relaxation in Matter* (Oxford Clarendon Press, 1979).
[17] M. Mehring, *Principles of High Resolution NMR in Solids*, 2nd ed. (Springer, Berlin, 1983).
[18] R. Kimmich, *NMR Tomography, Diffusometry, Relaxometry* (Springer, Berlin, 1997).
[19] A. Abragam, *The Principles of Nuclear Magnetism* (Oxford Clarendon Press, 1961).
[20] N. F. Fatkullin, T. Körber, and E. A. Rössler, Polymer **142**, 310 (2018).
[21] I. K. Ostrovskaya and N. F. Fatkullin, Polym. Sci., Ser. A **62**, 132 (2020).
[22] I. K. Ostrovskaya, N. F. Fatkullin, T. Körber, E. A. Rössler, A. Lozovoi, C. Mattea, and S. Stapf, J. Chem. Phys. **152**, 184904 (2020).
[23] M. Doi and S. F. Edwards, *The Theory of Polymer Dynamics* (Oxford Clarendon Press, 1989).
[24] A. Y. Grosberg and A. R. Khokhlov, *Statistical Physics of Macromolecules* (AIP Press, 1994).
[25] M. Rubinstein and R. H. Colby, *Polymer Physics* (Oxford University Press, 2003).
[26] P. G. de Gennes, *Scaling Concepts in Polymer Physics* (Cornell University Press, Ithaka, 1979).
[27] G. R. Strobl, *The Physics of Polymers* (Springer, 1997).
[28] N. Fatkullin and R. Kimmich, Phys. Rev. E **52**, 3273 (1995).
[29] R. C. Ball, P. T. Callaghan, and E. T. Samulski, J. Chem. Phys. **106**, 7352 (1997).
[30] T. N. Khazanovich, Polym. Sci. U.S.S.R. **4**, 727 (1963).
[31] R. Ullman, J. Chem. Phys. **43**, 3161 (1965).

[32]D. A. Markelov, M. Dolgushev, and E. Lähderanta, *Annual Reports on NMR Spectroscopy*, 1st ed. (Academic Press, 2017), Vol. 91, Chap. I, p. 1.
[33]M. Dolgushev, D. A. Markelov, F. Fürstenberg, and T. Guérin, Phys. Rev. E **94**, 012502 (2016).
[34]D. A. Markelov, F. Fürstenberg, and M. Dolgushev, Polymer **144**, 65 (2018).
[35]E. M. Pestryaev, Polym. Sci., Ser. A **62**, 766 (2020).
[36]E. M. Pestryaev, Polym. Sci., Ser. A **61**, 392 (2019).
[37]K. Lindt, C. Mattea, and S. Stapf (2022). "NMR Hahn echo decays in deuterated polyethylene oxide melts," Figshare, Dataset http://doi.org/10.6084/m9.figshare.19762933.
[38]L. J. Fetters, D. J. Lohse, and R. H. Colby, *Physical Properties of Polymers Handbook*, 2nd ed. (Springer, New York, 2007), Chap. XXV, p. 447.
[39]E. Fischer, R. Kimmich, U. Beginn, M. Möller, and N. Fatkullin, Phys. Rev. E **59**, 4079 (1999).
[40]D. G. Tsalikis, T. Koukoulas, V. G. Mavrantzas, R. Pasquino, D. Vlassopoulos, W. Pyckhout-Hintzen, A. Wischnewski, M. Monkenbusch, and D. Richter, Macromolecules **50**, 2565 (2017).
[41]O. Kratky and G. Porod, Recl. Trav. Chim. Pays-Bas **68**, 1106 (1949).
[42]H. Yamakava, *Modern Theory of Polymer Solutions* (Harper & Row, New York, 1974).
[43]E. A. Rössler, S. Stapf, and N. Fatkullin, Curr. Opin. Colloid Interface Sci. **18**, 173 (2013).
[44]K. S. Schweizer, J. Chem. Phys. **91**, 5802 (1989).
[45]K. S. Schweizer, J. Chem. Phys. **91**, 5822 (1989).
[46]K. S. Schweizer, M. Fuchs, G. Szamel, M. Guenza, and H. Tang, Macromol. Theory Simul. **6**, 1037 (1997).
[47]N. Fatkullin and R. Kimmich, J. Chem. Phys. **101**, 822 (1994).
[48]R. Kimmich, N. Fatkullin, H. W. Weber, and S. Stapf, J. Non-Cryst. Solids **172**, 689 (1994).
[49]M. A. Krutyeva, N. F. Fatkullin, and R. Kimmich, Polym. Sci., Ser. A **47**, 1022 (2005).
[50]N. Fatkullin, A. Gubaidullin, C. Mattea, and S. Stapf, J. Chem. Phys. **137**, 224907 (2012).